Direct analysis of particulate suspensions with inertia using the discrete Boltzmann equation

By CYRUS K. AIDUN†, YANNAN LU
AND E.-JIANG DING

Institute of Paper Science and Technology, 500 10th Street, N.W., Atlanta, GA 30318, USA

An efficient and robust computational method, based on the lattice-Boltzmann method, is presented for analysis of impermeable solid particle(s) suspended in fluid with inertia. In contrast to previous lattice-Boltzmann approaches, the present method can be used for any solid-to-fluid density ratio. The details of the numerical technique and implementation of the boundary conditions are presented. The accuracy and robustness of the method is demonstrated by simulating the flow over a circular cylinder in a two-dimensional channel, a circular cylinder in simple shear flow, sedimentation of a circular cylinder in a two-dimensional channel, and sedimentation of a sphere in a three-dimensional channel. With a solid-to-fluid density ratio close to one, new results from two-dimensional and three-dimensional computational analysis of dynamics of an ellipse and an ellipsoid in a simple shear flow, as well as two-dimensional and three-dimensional results for sedimenting ellipses and prolate spheroids, are presented.

1. Introduction

Many manufacturing processes involve transport of solid particles suspended in fluid in the form of slurries, colloids, polymers, or ceramics. For cases where the particle's inertia can be neglected, the dynamics of single-particle motion, interaction with other particles, and effects on the bulk properties are well understood. However, in many particle transport applications, the fluid and particle inertia cannot be neglected. In these cases, the effects of particle motion and particle–particle interaction on the micro-structure and the macroscopic transport behaviour are not well understood. In fact, very basic information, such as the effect of inertia on the interaction of two solid particles in a simple shear flow, is unavailable. In order to study the fundamental effect of inertia on particle motion, particle interaction and micro-structure, and effects on the bulk properties, we need to solve the full momentum equation to analyse the dynamics of individual particles suspended in the fluid. Progress has been made towards this goal by the recent finite element simulations of two-dimensional particles suspended in fluid by Hu, Crochet & Joseph (1992); Joseph (1994); Feng, Hu & Joseph (1994*a,b*); Huang, Feng & Joseph (1994), and Feng & Joseph (1995). These results provide considerable information on the particle motion and interaction at finite particle Reynolds number. Their finite element simulation is based on solution of the Navier–Stokes equation for the fluid domain using the commercial software, POLYFLOW. The procedure involves computation of the net force and torque

---

† Author to whom correspondence should be addressed.

on the solid particle, explicit translation and rotation of the particle, remeshing, and projection of the solution from the previous time step onto the re-meshed computational domain at every time step (Hu *et al.* 1992). To date, only two-dimensional solutions have been reported due to the excessive computational time required by this approach. Analysis of three-dimensional problems involving transport of solid particles requires a more efficient computational method.

The method presented here is based on the solution of the discrete Boltzmann equation for the fluid phase as it is coupled, through fluid–solid interaction rules, to the translation and rotation of the solid particles suspended in the fluid. The discrete Boltzmann equation treats the continuum fluid phase as a set of fluid particles which move in discrete directions. It is well established that with an appropriate equilibrium distribution function, the discrete Boltzmann equation will reduce to the full Navier–Stokes equation (McNamara & Zanetti 1988; Chen, Chen & Matthaeus 1992; Hou *et al.* 1995). The advantages of this approach are based on the local nature of the computations as well as the accuracy and robustness of the method. Numerical communications between the computational nodes are with immediate neighbours only and there is no need for solution of linear systems. Therefore, this method can be efficiently implemented on parallel processors, since the computational domain can be divided and distributed on many processors with little communication between each processor.

Application of the discrete Boltzmann method to analyse particles suspended in fluid was first proposed by Ladd, Colvin & Frenkel (1988) and Ladd (1994*a,b*). Ladd's model requires fluid to cross the boundary of the suspended solid particle and occupy the entire domain such that the computational nodes inside and outside the solid particle are treated in an identical manner. As Ladd (1994*a,b*) recognized, this method is limited to solid particles with density larger than the fluid density. This paper presents a method based on the discrete Boltzmann equation for analysis of suspended solid particles (Aidun, Lu & Ding 1997) with any solid-to-fluid density ratio. The present method works well for suspension flow with or without inertia for steady or unsteady flows. There is no need to change or adjust any parameters. Since there is no fluid to occupy the solid particle volume, fluid nodes appear and disappear as the solid particle moves through the domain. Therefore the computational algorithm is somewhat more involved than that of Ladd's model. However, if the number of solid particles in the system is not very large, the computational time for these two methods will be about the same.

The remaining part of this paper is organized as follows. In §2, the method is outlined in sufficient detail so that it can be easily programmed in any computer program language.† A series of comparisons with known solutions and experimental data is presented in §3 to demonstrate the accuracy and robustness of this approach. In §4 this method is used to simulate physical systems with solid-to-fluid density ratio close to one where other models do not apply. The results are compared with those of Jeffery (1922), for rotation of a two-dimensional ellipse and a three-dimensional ellipsoid in a shear flow at $Re \ll 1$. For sedimentation of ellipses in a channel (two-dimensional simulations), the results are compared to Feng & Joseph (1995) during the initial transient time. The computations are then extended to much longer times where new equilibrium periodic or stationary solutions are found. Also, new results for three-dimensional analysis of prolate spheroids for $Re_p = 2.26$ are presented. We close the paper with some concluding remarks in §5.

† The authors would be glad to provide the code for this method to interested readers upon their request.

k	σ	i	$e_{\sigma i}$	$\lvert e_{\sigma i}\rvert$	k	σ	i	$e_{\sigma i}$	$\lvert e_{\sigma i}\rvert$
0	0	1	(0, 0, 0)	0	9	2	5	(1, 0, 1)	$\sqrt{2}$
1	1	1	(1, 0, 0)	1	10	2	6	(0, 1, 1)	$\sqrt{2}$
2	2	1	(1, 1, 0)	$\sqrt{2}$	11	2	7	(−1, 0, 1)	$\sqrt{2}$
3	1	2	(0, 1, 0)	1	12	2	8	(0, −1, 1)	$\sqrt{2}$
4	2	2	(−1, 1, 0)	$\sqrt{2}$	13	1	5	(0, 0, 1)	1
5	1	3	(−1, 0, 0)	1	14	2	9	(−1, 0, −1)	$\sqrt{2}$
6	2	3	(−1, −1, 0)	$\sqrt{2}$	15	2	10	(0, −1, −1)	$\sqrt{2}$
7	1	4	(0, −1, 0)	1	16	2	11	(1, 0, −1)	$\sqrt{2}$
8	2	4	(1, −1, 0)	$\sqrt{2}$	17	2	12	(0, 1, −1)	$\sqrt{2}$
					18	1	6	(0, 0, −1)	1

TABLE 1. List of 19 velocities.

2. Method

2.1. *Discrete Boltzmann equation*

The lattice-Boltzmann equation (McNamara & Zanetti, 1988; Chen *et al.* 1992; Hou *et al.* 1995) is often written as

$$f_{\sigma i}(x + e_{\sigma i}, t + 1) - f_{\sigma i}(x, t) = -\frac{1}{\tau}[f_{\sigma i}(x, t) - f_{\sigma i}^{(0)}(x, t)], \tag{1}$$

where $f_{\sigma i}(x, t)$ represents the single-particle distribution function, $f_{\sigma i}^{(0)}(x, t)$ is the equilibrium distribution function, and τ is the single relaxation time. For the two-dimensional cases, a three-speed lattice-Boltzmann model is used where the fluid particles can be at rest or can move along the horizontal, vertical, and diagonal directions. Therefore the indices on the single-particle distribution function can only take values $\sigma = 0, i = 1$ or $\sigma = 1, 2, i = 1, \cdots, 4$. The velocity vectors are denoted as e_{01} for the fluid particles at rest, and e_{1i} and e_{2i} for the fluid particles moving along the non-diagonal and diagonal directions, respectively. The velocity vectors are defined as

$$e_{01} = (0, 0), \tag{2}$$

$$e_{1i} = \left(\cos\frac{i-1}{2}\pi, \sin\frac{i-1}{2}\pi\right), \quad i = 1, \cdots, 4, \tag{3}$$

$$e_{2i} = \sqrt{2}\left(\cos\left(\frac{i-1}{2}\pi + \frac{\pi}{4}\right), \sin\left(\frac{i-1}{2}\pi + \frac{\pi}{4}\right)\right), \quad i = 1, \cdots, 4, \tag{4}$$

where the value of i refers to each of the four diagonal or non-diagonal directions. In the three-dimensional analyses, the fluid phase is modelled by a group of fluid particles moving in a lattice with discrete velocities. In a three-dimensional domain, there are 19 different velocities which fall into three categories according to their magnitudes. Each category represent velocity vectors with the same magnitude but different directions. The velocity vectors are denoted $e_{\sigma i}$ with $\sigma = 0, 1, 2$, where 0 denotes the fluid particles that are at rest. Table 1 lists all 19 velocity vectors. At each time step, the moving fluid particles leave the original node and arrive at the nearest node along a given direction.

The density ρ and the macroscopic fluid velocity $\boldsymbol{u}$ are obtained from the first two moments, given by

$$\rho(\boldsymbol{x}, t) = \sum_{\sigma, i} f_{\sigma i}(\boldsymbol{x}, t), \quad \text{and} \quad \rho(\boldsymbol{x}, t)\boldsymbol{u}(\boldsymbol{x}, t) = \sum_{\sigma, i} f_{\sigma i}(\boldsymbol{x}, t)\boldsymbol{e}_{\sigma i}, \tag{5}$$

respectively. The collision term in (1) describes the change in $f_{\sigma i}$ due to instantaneous molecular collisions at the lattice nodes. The post-collision distribution function at $(\boldsymbol{x}, t_+)$ is

$$f_{\sigma i}(\boldsymbol{x}, t_+) = \boldsymbol{C} f_{\sigma i}(\boldsymbol{x}, t) \equiv f_{\sigma i}(\boldsymbol{x}, t) - \frac{1}{\tau}[f_{\sigma i}(\boldsymbol{x}, t) - f_{\sigma i}^{(0)}(\boldsymbol{x}, t)], \tag{6}$$

where t_+ is the time immediately after the collision, that is $t_+ - t \ll 1$. The operator $\boldsymbol{C}$ is called the 'collision' operator. After the collision, the post-collision distribution function $f_{\sigma i}$ is propagated for one time step, and the distribution function becomes

$$f_{\sigma i}(\boldsymbol{x} + \boldsymbol{e}_{\sigma i}, t+1) = f_{\sigma i}(\boldsymbol{x}, t_+).$$

It could be written in another form as

$$f_{\sigma i}(\boldsymbol{x}, t+1) = \boldsymbol{P}_0 f_{\sigma i}(\boldsymbol{x}, t_+) \equiv f_{\sigma i}(\boldsymbol{x} + \boldsymbol{e}_{\sigma i'}, t_+). \tag{7}$$

where $\boldsymbol{e}_{\sigma i'} = -\boldsymbol{e}_{\sigma i}$. The operator $\boldsymbol{P}_0$ in the above equation is referred to as the 'propagator'. In this paper $(\sigma i')$ always means the link with direction opposite to that of link (σi). Notice that total mass in the system is conserved under both operators $\boldsymbol{C}$ and $\boldsymbol{P}_0$. According to the lattice-Boltzmann equation (1), the distribution function at time $t+1$ can be calculated as

$$f_{\sigma i}(\boldsymbol{x}, t+1) = \boldsymbol{P}_0 \boldsymbol{C} f_{\sigma i}(\boldsymbol{x}, t). \tag{8}$$

In these simulations, $f_{\sigma i}^{(0)}(\boldsymbol{x}, t)$ is taken as

$$f_{\sigma i}^{(0)}(\boldsymbol{x}, t) = \rho(\boldsymbol{x})[A_\sigma + B_\sigma(\boldsymbol{e}_{\sigma i} \cdot \boldsymbol{u}) + C_\sigma(\boldsymbol{e}_{\sigma i} \cdot \boldsymbol{u})^2 + D_\sigma u^2], \tag{9}$$

where $\rho(\boldsymbol{x})$ is the fluid particle density at node $\boldsymbol{x}$. For the resting particles, $B_0 = C_0 = 0$ from the symmetry consideration. The constraints for $f_{\sigma i}^{(0)}$ are as follows:

$$\sum_\sigma \sum_i f_{\sigma i}^{(0)} = \rho, \tag{10}$$

$$\sum_\sigma \sum_i f_{\sigma i}^{(0)} \boldsymbol{e}_{\sigma i} = \rho \boldsymbol{u}, \tag{11}$$

and

$$\sum_\sigma \sum_i f_{\sigma i}^{(0)} \boldsymbol{e}_{\sigma i} \boldsymbol{e}_{\sigma i} = c_s^2 \rho \boldsymbol{I} + \rho \boldsymbol{u} \boldsymbol{u}, \tag{12}$$

where c_s is the speed of sound and $\boldsymbol{I}$ denotes the unit tensor.

In the two-dimensional case, (10) gives

$$A_0 + 4A_1 + 4A_2 + 2C_1 + 4C_2 + D_0 + 4D_1 + 4D_2 = 1.$$

Equation (11) gives

$$2B_1 + 4B_2 = 1.$$

From (12) four independent constraints may be obtained. In fact, the trace of both sides gives $2(2A_1 + 4A_2) + (2C_1 + 8C_2 + 4D_1 + 8D_2)u^2 = 2c_s^2 + u^2$, which means that

$$2A_1 + 4A_2 = c_s^2,$$

and
$$2C_1 + 8C_2 + 4D_1 + 8D_2 = 1.$$
The u_x^2 component of (12) gives
$$2C_1 + 4C_2 + 2D_1 + 4D_2 = 1,$$
and the $u_x u_y$ component of (12) gives
$$8C_2 = 1.$$
The final constraint comes from the isotropy of the non-equilibrium part of the momentum flux. It turns out to be
$$2B_1 - 8B_2 = 0.$$
From these constraints the coefficients in (9) can be obtained as

$$\left. \begin{aligned} &B_0 = 0, \quad C_0 = 0, \\ A_1 = \tfrac{1}{2}(1 - A_0 - c_s^2), \quad &B_1 = \tfrac{1}{3}, \quad C_1 = \tfrac{1}{2}, \quad D_1 = -\tfrac{1}{2}(1 + D_0), \\ A_2 = -\tfrac{1}{4}(1 - A_0 - 2c_s^2), \quad &B_2 = \tfrac{1}{12}, \quad C_2 = \tfrac{1}{8}, \quad D_2 = \tfrac{1}{8}(1 + 2D_0). \end{aligned} \right\} \quad (13)$$

When $c_s^2 = 1/3$, $D_0 = 0$ and $A_0 = 1/2$, the coefficients are given by

$$\left. \begin{aligned} A_0 = \tfrac{1}{2}, \quad &B_0 = 0, \quad C_0 = 0, \quad D_0 = 0, \\ A_1 = \tfrac{1}{12}, \quad &B_1 = \tfrac{1}{3}, \quad C_1 = \tfrac{1}{2}, \quad D_1 = -\tfrac{1}{2}, \\ A_2 = \tfrac{1}{24}, \quad &B_2 = \tfrac{1}{12}, \quad C_2 = \tfrac{1}{8}, \quad D_2 = \tfrac{1}{8}. \end{aligned} \right\} \quad (14)$$

For this model, the kinematic viscosity is given by $v = (2\tau - 1)/6$ (Hou *et al.* 1995).

The constants for the equilibrium distribution function, $f_{\sigma i}^{(0)}(x, t)$, in three-dimensional applications are given by

$$\left. \begin{aligned} A_0 = \tfrac{1}{4}, \quad &B_0 = 0, \quad C_0 = 0, \quad D_0 = 0, \\ A_1 = \tfrac{1}{12}, \quad &B_1 = \tfrac{1}{6}, \quad C_1 = \tfrac{1}{4}, \quad D_1 = -\tfrac{1}{4}, \\ A_2 = \tfrac{1}{48}, \quad &B_2 = \tfrac{1}{12}, \quad C_2 = \tfrac{1}{8}, \quad D_2 = 0. \end{aligned} \right\} \quad (15)$$

The parameter c_s and kinematic viscosity have the same values as for the two-dimensional case defined above.

2.2. *Boundary conditions*

The lattice-Boltzmann operators must be modified at the boundaries to incorporate the boundary conditions. Two different boundary conditions are discussed in this section. These are the no-slip wall and the stress-free conditions. The second boundary condition is useful for simulation of particle transport or sedimentation in infinite fluid channels. For example, in sedimentation problems it is natural to assume a stress-free boundary condition at the outlet and a constant velocity at the inlet as the computational domain moves with the particle.

The no-slip wall boundary condition has been discussed by Ladd (1994*a,b*). Assume that fluid node x is a boundary node adjacent to the stationary no-slip wall. The links at x are divided into two groups, boundary links (BL) and fluid links (FL). The wall is always assumed to be located at the middle of the boundary links. The no-slip rule is imposed at all boundary nodes adjacent to the wall. For a stationary solid surface,

(7) as applied to the boundary nodes should be modified. As mentioned above, $(\sigma i')$ always means the link with direction opposite to that of link (σi). When $(\sigma i')$ is a boundary link, there would be no fluid node at $x + e_{\sigma i'}$. In this case, the component $f_{\sigma i}(x, t+1)$ is obtained by bouncing back the component $f_{\sigma i'}(x, t_+)$. When $(\sigma i')$ is not a boundary link, (7) is applicable. Hence

$$f_{\sigma i}(x, t+1) = \boldsymbol{P}_{n-s}(\boldsymbol{0}) f_{\sigma i}(x, t_+) \equiv \begin{cases} f_{\sigma i'}(x, t_+), & \text{if } (\sigma i') \text{ is BL}, \\ f_{\sigma i}(x + e_{\sigma i'}, t_+), & \text{otherwise}, \end{cases} \tag{16}$$

where $\boldsymbol{P}_{n-s}(\boldsymbol{0})$ is called the no-slip propagator for a stationary wall. Then the distribution function at these boundary nodes should be

$$f_{\sigma i}(x, t+1) = \boldsymbol{P}_{n-s}(\boldsymbol{0}) \boldsymbol{C} f_{\sigma i}(x, t). \tag{17}$$

Notice that $\boldsymbol{P}_{n-s}(\boldsymbol{0})$ is also a mass conserved operator.

If the no-slip wall is moving with a velocity u_b, the fluid adjacent to the wall must move with the same velocity. For all boundary nodes, that is nodes with one or more boundary links, the no-slip boundary condition operator, $\boldsymbol{P}_{n-s}(u_b)$, is defined as (Ladd 1994*a,b*)

$$f_{\sigma i}(x, t+1) = \boldsymbol{P}_{n-s}(u_b) f_{\sigma i}(x, t_+) \equiv \begin{cases} f_{\sigma i'}(x, t_+) + 2\rho B_\sigma u_b \cdot e_{\sigma i}, & \text{if } (\sigma i') \text{ is BL} \\ f_{\sigma i}(x + e_{\sigma i'}, t_+), & \text{otherwise}. \end{cases} \tag{18}$$

The density at node x at time $t+1$, $\rho = \rho(x, t+1)$, is given by

$$\rho = \sum_{\sigma i} \boldsymbol{P}_{n-s}(u_b) f_{\sigma i}(x, t_+) = \sum_{\sigma i} \boldsymbol{P}_{n-s}(\boldsymbol{0}) f_{\sigma i}(x, t_+) + \sum_{\sigma i' \in BL} 2\rho B_\sigma u_b \cdot e_{\sigma i}.$$

Hence

$$\rho = \frac{\sum_{\sigma i} \boldsymbol{P}_{n-s}(\boldsymbol{0}) f_{\sigma i}(x, t_+)}{1 - \sum_{\sigma i' \in BL} 2 B_\sigma u_b \cdot e_{\sigma i}}.$$

If the wall moves tangentially, the summation

$$\sum_{\sigma i' \in BL} B_\sigma u_b \cdot e_{\sigma i} = 0$$

and the operator $\boldsymbol{P}_{n-s}(u_b)$ is mass conserved. However, if the velocity u_b a has non-zero normal component, the operator is not mass conserved.

The distribution function at these nodes should be

$$f_{\sigma i}(x, t+1) = \boldsymbol{P}_{n-s}(u_b) \boldsymbol{C} f_{\sigma i}(x, t). \tag{19}$$

Stress-free boundary conditions are an effective method to simulate problems with an infinitely large fluid domain. In many problems, although the fluid domain is infinitely large, there is a finite region with a non-zero velocity gradient where convective and viscous forces are significant. Cross-flow over an object or sedimentation of a solid particle in an infinitely long channel are two examples. In the first case where the particle is stationary, boundary conditions are imposed on a fixed computational domain, with a constant velocity boundary condition at the upstream boundary and a stress-free boundary condition imposed at the downstream boundary far from the object. In the second case where the particle is free to move, a stationary computational domain may not always be the most computationally efficient approach. In some cases

it is more efficient to move the computational domain in such a way as to accurately capture the physics of the fluid flow and particle dynamics without the need for an exceedingly large domain. An example is one or more solid particles released in an infinitely long channel. The particles travel a long distance from their initially released position before settling into an equilibrium state. Moving the computational domain requires a net flow of fluid through the domain. This section outlines the method of imposing a stress-free boundary condition on a moving computational domain about a particle sedimenting in an infinite channel. The same method can be used for similar problems, such as particle transport in pressure-driven or shear-driven flows.

For simplicity, relative to the particle, the downstream side is set at the right-hand end of the system, $x = x_{max}$; the upstream side is set at the left-hand end, $x = 0$; and the constant velocity $\boldsymbol{u}_1$ of the fluid on the upstream side is directed to right. Also, the particle is assumed to be settling toward the left direction. The pre-modified distribution operator, given as

$$\tilde{f}_{\sigma i}(\boldsymbol{x}, t + 1) = \boldsymbol{P}_{n-s}(\boldsymbol{0})f_{\sigma i}(\boldsymbol{x}, t_+),$$

is first applied to the downstream and the upstream boundaries at $\boldsymbol{x} = (x_{max}, y)$ and $\boldsymbol{x} = (0, y)$, respectively.

The downstream side (i.e. the outlet) is stress-free, meaning

$$\frac{\partial u_x}{\partial x} = 0 \quad \text{at} \quad x = x_{max}.$$

A stress-free operator, $\boldsymbol{P}_{s-f}$, is defined as

$$f_{\sigma i}(\boldsymbol{x}, t + 1) = \boldsymbol{P}_{s-f}f_{\sigma i}(\boldsymbol{x}, t_+) \equiv \begin{cases} \tilde{f}_{\sigma i}(\boldsymbol{x}', t + 1), & \text{if } (\sigma i') \text{ is BL} \\ \tilde{f}_{\sigma i}(\boldsymbol{x}, t + 1) + \delta f(\boldsymbol{x}, t + 1), & \text{if } \sigma = 0 \\ \tilde{f}_{\sigma i}(\boldsymbol{x}, t + 1), & \text{otherwise,} \end{cases} \tag{20}$$

where $\boldsymbol{x}' = (x_{max} - 1, y)$, $\delta f(\boldsymbol{x}, t + 1)$ is defined below.

At the upstream side, a constant velocity, $\boldsymbol{u}_1$, normal to the boundary is imposed by applying (18). For the upstream boundary, the boundary condition is given by

$$f_{\sigma i}(\boldsymbol{x}, t + 1) = \boldsymbol{P}_{n-s}(\boldsymbol{u}_1)f_{\sigma i}(\boldsymbol{x}, t_+) \equiv \begin{cases} \tilde{f}_{\sigma i}(\boldsymbol{x}, t + 1) + 2\rho B_\sigma u_1, & \text{if } (\sigma i') \text{ is BL} \\ \tilde{f}_{\sigma i}(\boldsymbol{x}, t + 1), & \text{otherwise.} \end{cases} \tag{21}$$

The total flux at each boundary node at the upstream boundary is given by

$$w = \sum_{(\sigma i') \in BL} 2\rho B_\sigma u_1 = \rho u_1,$$

where

$$\rho = \rho(\boldsymbol{x}, t + 1) = \frac{\displaystyle\sum_{\sigma i} \tilde{f}_{\sigma i}(\boldsymbol{x}, t + 1)}{1 - \displaystyle\sum_{(\sigma i') \in BL} 2B_\sigma u_1}.$$

In order to keep the total mass in the system unchanged, the term $\delta f(\boldsymbol{x}, t + 1)$ in (20) should be

$$\delta f(\boldsymbol{x}, t + 1) = \sum_{(\sigma i') \in BL} [\tilde{f}_{\sigma i}(\boldsymbol{x}, t + 1) - f_{\sigma i}(\boldsymbol{x}', t + 1)] - w.$$

Then the calculation at the downstream and upstream (i.e. outlet and inlet, respectively) boundary nodes should be carried out as

$$f_{\sigma i}(\boldsymbol{x}, t+1) = \boldsymbol{P}_{s-f}\boldsymbol{C}f_{\sigma i}(\boldsymbol{x}, t), \quad \boldsymbol{x} = (x_{max}, y), \tag{22}$$

and

$$f_{\sigma i}(\boldsymbol{x}, t+1) = \boldsymbol{P}_{n-s}(\boldsymbol{u}_1)\boldsymbol{C}f_{\sigma i}(\boldsymbol{x}, t), \quad \boldsymbol{x} = (0, y), \tag{23}$$

respectively. In this simulation, as soon as the particle shifts by one lattice unit, we move the computational domain by one lattice unit. This is done by removing one layer of fluid nodes at the downstream side of the system and adding one layer of lattice nodes to the upstream side. In this way, the computational domain captures the relevant section of the infinite domain inside the channel.

2.3. *Solid particle boundary interaction and dynamics*

It is more difficult to deal with the interaction between fluid and a moving solid particle than that between fluid and a stationary solid wall. The reason is that a solid particle can move by both translation and rotation. In the lattice-Boltzmann simulation of suspension flows, the solid particles move in a continuous way based on the Newtonian dynamics principles. The position of the solid particles will always be updated accurately. However, when the interactions between solid particles and fluid are discussed, the solid boundary is always assumed to be at the midpoint of the boundary nodes. The fluid nodes with at least one link connecting to a solid node are called the fluid-boundary nodes. In two-dimensional cases, a fluid-boundary node may have a total number 1 to 5 no-slip links to the boundary of a solid particle.

The boundary condition imposed at the solid–fluid interface is the no-slip condition; that is, the fluid adjacent to the solid surface moves at the same velocity as the solid surface. In this case, the fluid particles impact the solid boundary in the middle of the convection process and exchange momentum with the solid particle. Ladd (1994*a,b*) provides a relation for the exchange of momentum between the fluid and the solid boundary nodes. As mentioned before, he assumes that the fluid particles can occupy the entire domain including the volume of the solid particle. The fluid inside the solid particle exerts a time-dependent force on the solid particle based on the particle's inertia which is influenced by the fluid inertia inside the particle. Some improvement on Ladd's method for updating the equations of motion has been described (Lowe, Frenkel & Masters 1995).

We have developed a method which does not require transfer of fluid into the solid particle and, therefore, applies to real suspensions (Aidun & Lu 1995; Aidun *et al.* 1997). In this method, the force on the solid particle consists of the body force and the hydrodynamic force exerted on the surface from the nodes outside the solid boundary which are occupied by fluid. The nodes inside the solid boundary are solid nodes and, therefore, contain no fluid. Consequently, the transfer of momentum is only between the solid boundary and the adjacent fluid.

The calculation of the boundary node distribution function in the lattice-Boltzmann method consists of three operators:

1. collision at the lattice node $\boldsymbol{x}$:

$$f_{\sigma i}(\boldsymbol{x}, t_+) = \boldsymbol{C}f_{\sigma i}(\boldsymbol{x}, t), \tag{24}$$

which is the same as (6);

2. no-slip rule:

$$\tilde{f}_{\sigma i}(\boldsymbol{x}, t+1) = \boldsymbol{P}_{n-s}(0)f_{\sigma i}(\boldsymbol{x}, t_+), \tag{25}$$

which is the same as (16);

3. modification of the magnitude of the distribution function components:

$$f_{\sigma i}(x, t+1) = P_{n-s}(u_b)f_{\sigma i}(x, t_+) \equiv \begin{cases} \tilde{f}_{\sigma i}(x, t+1) + 2\rho B_\sigma u_b \cdot e_{\sigma i}, & \text{if } (\sigma i') \text{ is BL} \\ \tilde{f}_{\sigma i}(x, t+1), & \text{otherwise.} \end{cases} \quad (26)$$

Note that (26) has the same form as (18); and it is applied with the following computational algorithm. First, u_b is obtained from the position vector of the centre of mass, $X(t)$, the translational velocity, $U(t)$, and the angular velocity, $\Omega(t)$, of the solid particle, that is

$$u_b = U(t) + \Omega(t) \times [x + \tfrac{1}{2}e_{\sigma i'} - X(t)].$$

Secondly, the density at node x in this case can change. In fact, since

$$\rho = \rho(x, t+1) = \sum_{\sigma i} f_{\sigma i}(x, t+1)$$

and

$$\tilde{\rho} = \tilde{\rho}(x, t+1) = \sum_{\sigma i} \tilde{f}_{\sigma i}(x, t+1),$$

we have that

$$\rho(x, t+1) = \frac{\tilde{\rho}(x, t+1)}{1 - 2 \sum_{(\sigma i') \in BL} B_\sigma u_b \cdot e_{\sigma i}}. \quad (27)$$

The distribution function at the fluid-boundary nodes should be calculated as

$$f_{\sigma i}(x, t+1) = P_{n-s}(u_b)C f_{\sigma i}(x, t). \quad (28)$$

The fluid-boundary node then has an increment of momentum

$$\delta p_{\sigma i} = \begin{cases} 2e_{\sigma i}[f_{\sigma i}(x, t+1) - \rho(x, t+1)B_\sigma u_b \cdot e_{\sigma i}], & \text{if } (\sigma i') \text{ is BL} \\ 0, & \text{otherwise,} \end{cases}$$

and an impulse force exerted on the particle for any boundary link $(\sigma i')$ is given by

$$F_{\sigma i}^{(b)}(x + \tfrac{1}{2}e_{\sigma i'}, t + \tfrac{1}{2}) = -\delta p_{\sigma i}/\Delta t.$$

We treat the force as if it were applied uniformly on the solid particle in time interval from t to $t+1$, therefore

$$F_{\sigma i}^{(b)}(x + \tfrac{1}{2}e_{\sigma i'}, t + \tfrac{1}{2}) = 2e_{\sigma i'}[f_{\sigma i}(x, t+1) + \rho(x, t+1)B_\sigma u_b \cdot e_{\sigma i'}], \quad (29)$$

The torque, $T_{\sigma i}^{(b)}$, with respect to the centre of mass, X, is given by

$$T_{\sigma i}^{(b)}(x + \tfrac{1}{2}e_{\sigma i'}, t + \tfrac{1}{2}) = [x + \tfrac{1}{2}e_{\sigma i'} - X(t)] \times F_{\sigma i}^{(b)}(x + \tfrac{1}{2}e_{\sigma i'}, t + \tfrac{1}{2}). \quad (30)$$

2.4. *Dynamics of particles suspended in fluid*

The method to advance the system through one time step is outlined in this section.

As the solid particle moves during the time interval $t_0 - 1$ to t_0, it may cover some fluid nodes. At the time a fluid node is covered by a solid particle, the particle will assume the momentum of the fluid node, hence a small impulse force is applied to the solid particle. By distributing the force through the time interval $\Delta t = 1$, the force

is given by

$$F^{(c)}(x, t_0 + \tfrac{1}{2}) = \sum_{\sigma i} f_{\sigma i}(x, t_0) e_{\sigma i},$$ (31)

and the torque on the solid particle is given by

$$T^{(c)}(x, t_0 + \tfrac{1}{2}) = [x - X(t_0)] \times F^{(c)}(x, t_0 + \tfrac{1}{2}).$$ (32)

The density for a new fluid node, uncovered due to the motion of the solid particle, is obtained with the following relation:

$$\rho(x, t_0) = \frac{1}{N_b} \sum_{N_b} \rho(x + e_{\sigma i'}, t_0),$$ (33)

where x is the new boundary node and N_b is the number of nodes adjacent to the uncovered boundary node. This relation states that the fluid particle density of the new node is equal to the average fluid particle density of its nneighbouring nodes. The macroscopic velocity of the new boundary node is equal to the solid boundary node at the time step when it is uncovered, that is

$$u(x, t_0) = U(t_0) + \Omega(t_0) \times [x - X(t_0)].$$ (34)

These values are used in (9) to compute the equilibrium distribution function $f_{\sigma i}^{(0)}(x, t_0)$ for the newly uncovered boundary node. Since the newly created fluid node carried a total amount of momentum equal to $\rho(x, t_0)u(x, t_0)$, the solid particle must lose the same amount of momentum. Hence, the force and torque, given respectively by

$$F^{(u)}(x, t_0 + \tfrac{1}{2}) = -\rho(x, t_0)u(x, t_0)$$ (35)

and

$$T^{(u)}(x, t_0 + \tfrac{1}{2}) = [x - X(t_0)] \times F^{(u)}(x, t_0 + \tfrac{1}{2}),$$ (36)

are exerted on the suspended particle.

The force and the torque on the solid particle exerted by the fluid-boundary nodes, are obtained from (31) and (32). Then, total force and torque on the solid particle at time $t_0 + 1/2$ are given by

$$F(t_0 + \tfrac{1}{2}) = \sum_{FBN} \sum_{\sigma i} F_{\sigma i}^{(b)}(x + \tfrac{1}{2}e_{\sigma i'}, t_0 + \tfrac{1}{2}) + \sum_{CN} F^{(c)}(x, t_0 + \tfrac{1}{2}) + \sum_{UN} F^{(u)}(x, t_0 + \tfrac{1}{2}),$$ (37)

and

$$T(t_0 + \tfrac{1}{2}) = \sum_{FBN} \sum_{\sigma i} T_{\sigma i}^{(b)}(x + \tfrac{1}{2}e_{\sigma i'}, t_0 + \tfrac{1}{2}) + \sum_{CN} T^{(c)}(x, t_0 + \tfrac{1}{2}) + \sum_{UN} T^{(u)}(x, t_0 + \tfrac{1}{2}),$$ (38)

respectively, where FBN stands for the fluid-boundary nodes, CN for the covered nodes, and UN for uncovered nodes, respectively. The total force and torque at time t_0 are averaged by those at time $t_0 - 1/2$ and $t_0 + 1/2$, that is

$$F(t_0) = \tfrac{1}{2}[F(t_0 + \tfrac{1}{2}) + F(t_0 - \tfrac{1}{2})],$$ (39)

and

$$T(t_0) = \tfrac{1}{2}[T(t_0 + \tfrac{1}{2}) + T(t_0 - \tfrac{1}{2})].$$ (40)

With the net force and the torque calculated from the above equations, the motion of the solid particle from $t = t_0$ to $t = t_0 + 1$ is determined by solving Newton's equations by

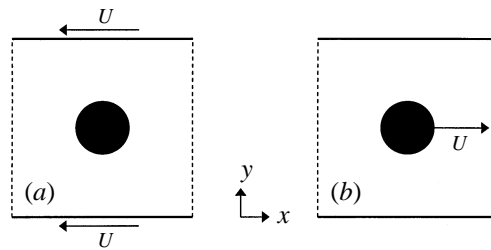$$M\frac{\mathrm{d}U(t)}{\mathrm{d}t} = F(t_0),$$ (41)

FIGURE 1. A circular particle moves along the centreline of a straight channel. (*a*) The coordinate system is fixed with the cylinder while the top and bottom walls move with a constant velocity. (*b*) The particle moves at a constant velocity while the walls are stationary.

for translation, and

$$\boldsymbol{I} \cdot \frac{\mathrm{d}\Omega(t)}{\mathrm{d}t} + \Omega(t) \times [\boldsymbol{I} \cdot \Omega(t)] = \boldsymbol{T}(t_0), \tag{42}$$

for rotation of the solid particles. Here M is the mass of the suspended particle, $\boldsymbol{I}$ is the inertial tensor, and Ω is the angular velocity. Notice that in (42) the derivative $\mathrm{d}\Omega/\mathrm{d}t$ is dependent on Ω, and therefore a simple Euler integration procedure may not give accurate results. In this simulation, these equations are solved using a fourth-order accurate Runge–Kutta integration procedure to obtain the complete motion of the suspended solid particles in the fluid. The simpler approach presented above can be applied to a wider range of parameters than the method presented by Ladd (1994*a,b*), is more robust, and is also an improvement over the earlier method presented by Aidun & Lu (1995)

3. Application

In this section the method presented above is examined and validated by application to four cases with known solutions.

3.1. *Flow over a circular cylinder in a channel* (*two-dimensional*)

A circular cylinder moves along the centreline of a channel with velocity U, as shown in figure 1. To solve for the velocity and pressure profile, one can either fix the coordinate system on the cylinder (figure 1*a*) or the wall (figure 1*b*). The Navier–Stokes equations, being Galilean invariant, give exactly the same velocity and pressure profiles for these two cases. To demonstrate Galilean invariance with the new lattice-Boltzmann approach presented above, we simulate this problem in both frames of reference.

The computational domain is 64×64 lattice units. Periodic boundary conditions are applied at the sides of the domain and no-slip conditions are imposed along the solid surfaces. The diameter d of the cylinder is 8.0, and the particle Reynolds number, Re_p, defined as Ud/v is 1.

These two cases are solved with the discrete Boltzmann equation using the method outlined in the present paper. The results for the velocity profile and the pressure distribution along the surface of the cylinder for each case are presented in figures 2 and 3, respectively. There is perfect agreement for the solution of the two cases showing that the solid–fluid boundary rule for moving objects, outlined above, gives the same result as the solution of the Boltzmann equation for stationary boundaries.
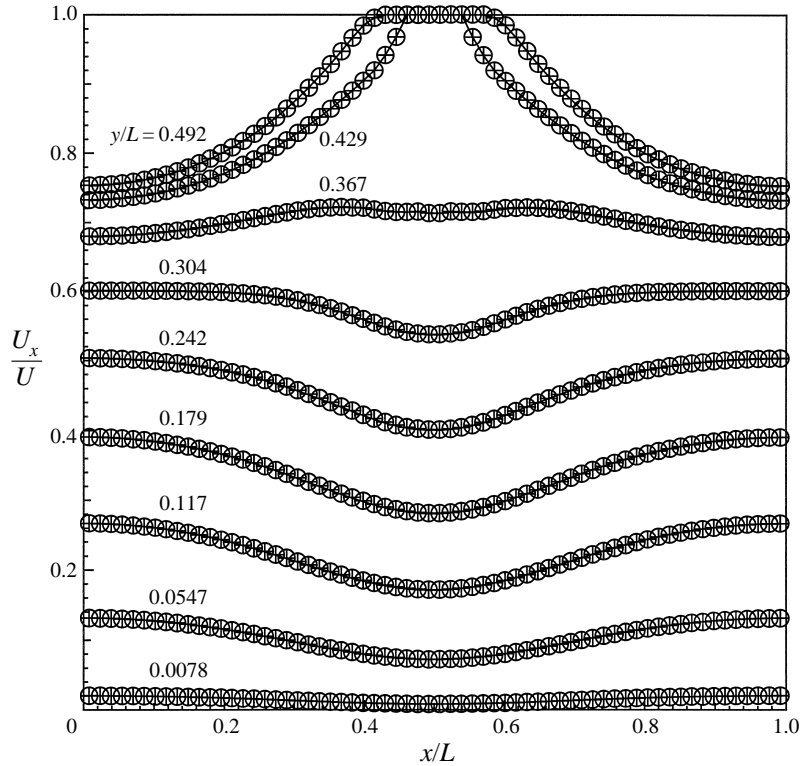
FIGURE 2. *X*-component of velocity field along horizontal lines: +, the present model applied to the moving cylinder; ○, Ladd's model. The Galilean transformed results for the case of the fixed particle are presented by the solid lines.

Since the flow is steady state, the results from the present method are the same as the results obtained with Ladd's (1994*a,b*) method.

3.2. *Circular cylinder suspended in Couette flow*

A circular cylinder is located in the middle of a straight channel, where both walls move in opposite directions. If the centre of the particle is on the centreline, then the particle should only rotate without drifting off the centreline. The second case is when the top wall moves while the bottom wall is stationary, and the particle at the centreline is moving with the average velocity of both walls. Although these two cases are identical, in numerical simulations of the second case, due to the round-off errors, the particle might slightly drift away from the centreline. A good model should give small vertical drift, and this drift should become negligible as the lattice size decreases and numerical resolution increases. Assume that ΔU is the relative velocity of the two walls, and L is the distance between them. In the simulation, the size of the domain is $2L \times L$. In shear flow, the Reynolds number is defined as $Re = Gd^2/v$, where d is the diameter of the particle, and $G = \Delta U/L$ is the shear rate. Results from Ladd's method are included as well. Results from the present method for three different sizes of systems or Reynolds numbers are shown in figure 4. In all three situations, it can be seen that the vertical drift of the particle is very small and within expected numerical resolution.
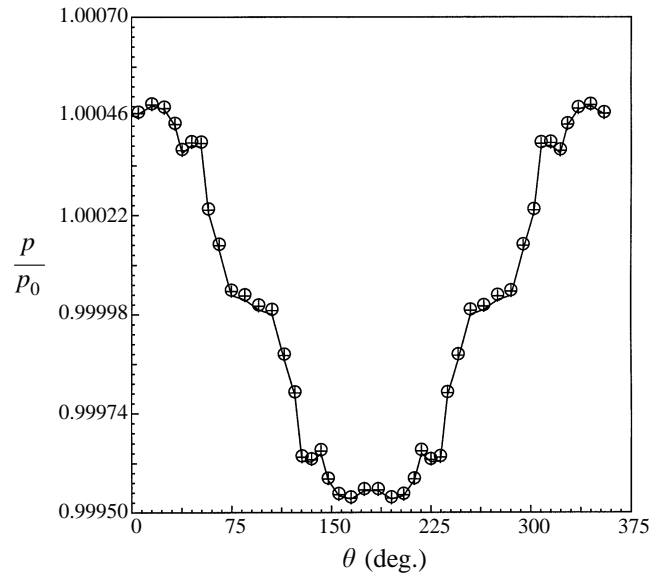
FIGURE 3. Angular distribution of the pressure at the interface relative to the undisturbed pressure. The angle in degrees is measured from the front of the particle: +, the present model; ○, Ladd's model. The results for the case of the fixed particle are presented by the solid line.
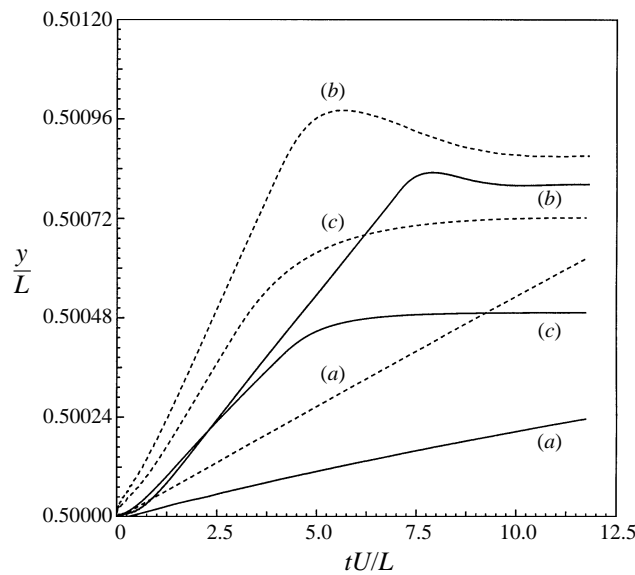

FIGURE 4. Lateral motion of a circular particle in an asymmetrical Couette channel where the bottom wall is stationary. The solid lines are for the results of the present model. The dashed lines are for Ladd's model. (a) $Re_p = 0.8649$, $d = 24.8$, $L = 64$; (b) $Re_p = 8.4677$, $d = 50.8$, $L = 128$; and (c) $Re_p = 8.4677$, $d = 98.8$, $L = 256$.
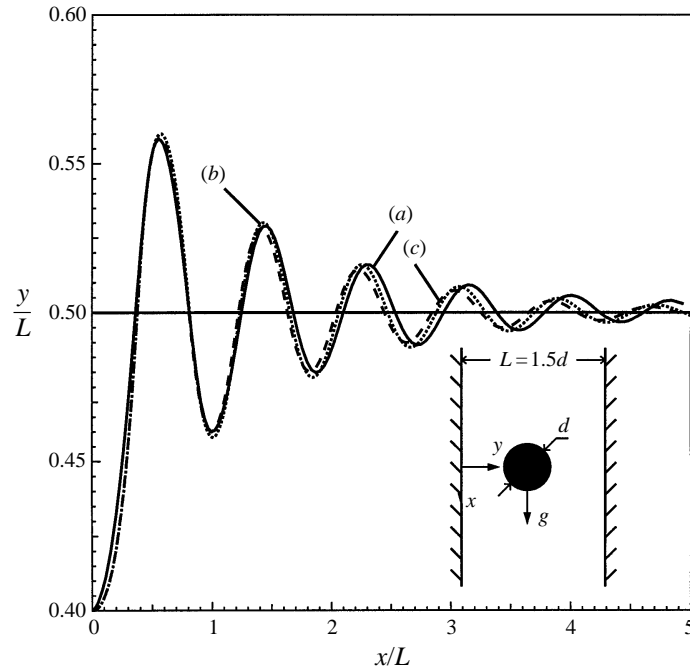
FIGURE 5. Settling trajectory of a circular particle in a vertical channel. Comparison between two different lattice-Boltzmann models and the simulation results of Feng *et al.* 1994 are presented: (*a*) Feng *et al.*; (*b*) the present lattice-Boltzmann method; and (*c*) Ladd's (1994*a,b*) method allowing fluid inside the solid particle. The results based on Ladd's method are obtained with the necessary density correction, as outlined by Ladd (1994*a,b*). The particle Reynolds numbers are 6.283 for (*a*), and 6.759 for (*b,c*).

3.3. *Sedimentation of a circular cylinder in a channel* (*two-dimensional*)

The sedimentation of a single circular particle in a narrow channel is considered in this section. Recently, Feng *et al.* (1994*a*) have simulated this problem by directly solving the Navier–Stokes equation for the fluid, and the Newtonian dynamics equation for the solid particle. They found that at a certain Reynolds number interval, the particle enters a damped oscillation and then asymptotically reaches steady state.

The same conditions as in Feng *et al.* (1994*a*) are used in the present analysis. That is, a circular particle of diameter d is released in a vertical channel of width $L = 1.5d$ and then settles under gravity. The initial position of the particle is off the centreline of the channel. The density ratio of solid to fluid is 1.3. The inlet of the domain, where zero velocity is applied uniformly, is always $10d$ from the upstream side of the moving particle, whereas the downstream boundary is $15d$ from the particle. The normal derivative of velocity is set to zero at the downstream boundary, as outlined in §2.2. In the present simulation, $d = 120$, $\tau = 0.8634$, and the size of the domain is 3000×180 lattice nodes. The particle Reynolds number is based on the diameter and the terminal velocity of the solid particle. The results show that the particle drifts away from the wall and oscillates about the centreline, as shown in figure 5, until it reaches the equilibrium position along the centreline. The results of Feng *et al.* (1994*a*) are also plotted for comparison. Since the density ratio of solid to fluid is 1.3, larger than one, application of the lattice-Boltzmann shell model with fluid inside the solid particle (Ladd 1994*a,b*) to this problem would also give accurate results.
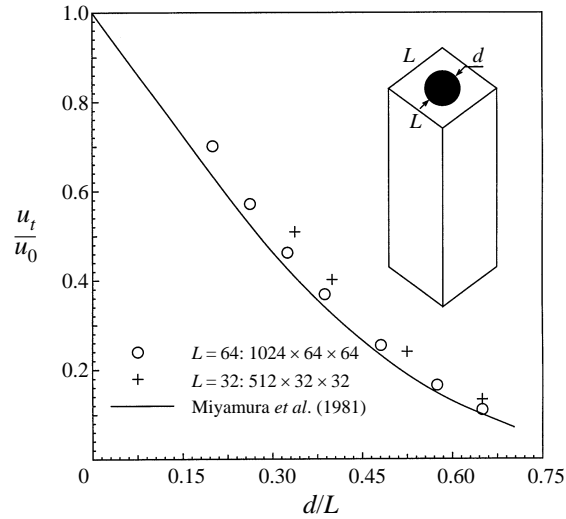
FIGURE 6. Wall effect on a single sphere settling in a long square channel. The solid line is a best fit to the experimental data of Miyamura *et al.* The open circles and + symbols are from our lattice-Boltzmann computational analysis. The results are within the experimental error.

3.4. *Sedimentation of a sphere in a channel* (*three-dimensional*)

A spherical particle of diameter d is released in a vertical square channel of width L which then settles under gravity. The sphere is initially released at the centre of the cross-section of the channel with zero velocity. The particle settles along the axis of the channel and reaches its terminal velocity. With the walls at a finite distance from the particle, the terminal velocity will be less than the terminal velocity of an unconfined particle. Aidun & Lu (1995) have analysed the two-dimensional version of this problem for $0 < Re < 3.3$ and compared their results with the numerical results of Feng *et al.* (1994*a*,*b*) with perfect agreement in all cases. Here results from analysis of the three-dimensional problem are presented and compared with the experiments of Miyamura, Iwasaki & Ishii (1981). We have not been able to find any other three-dimensional computational simulations of this problem. With the new model, the lattice-Boltzmann simulation has been carried out for the three-dimensional sedimentation in the same conditions as the experiments. In the present analysis, the channel is divided into $1024 \times 64 \times 64$ lattice units. The inlet of the domain where zero velocity is applied uniformly is always 400 lattice units away from the particle, whereas the downstream boundary is 624 lattice units downstream from the particle. The normal derivative of velocity is set to zero at the downstream boundary. In this simulation the range of the particle Reynolds number is from 0.2 to 0.6, and the solid-to-fluid density ratio is $\alpha = 2$. Results from a coarser grid, $512 \times 32 \times 32$, are also included for evaluating the effect of computational resolution. The wall effect is defined as

$$\xi = u_t/u_0,$$

where u_t is the terminal velocity with nearby boundary walls, and u_0 is the unconfined terminal velocity from Stokes equation. Figure 6 shows a comparison of the results from our computational analysis with the best curve fit to the experimental data of Miyamura *et al.* (1981). As shown in this figure, there is good agreement between the experiments and our computational results.

4. Application to solid particles with density ratio close to one

Cases where the density ratio of solid to fluid is close to one or less than one cannot be investigated by previous methods (e.g. Ladd 1994*a,b*). However, the present method can be used for any density ratio. Results for various cases, where the solid-to-fluid density ratio is 1.003, are provided in this section.

4.1. *Rotation of an ellipse in a simple shear flow*

The motion of a solid ellipsoid

$$\frac{x^2}{a^2} + \frac{y^2}{b^2} + \frac{z^2}{c^2} = 1 \tag{43}$$

in a simple shear flow is analysed in this section. Jeffery (1922) studied the motion at vanishing Reynolds number and obtained analytical solutions for two special cases. He assumed the force and torque on the particle to be zero. One of the special cases is that when one of the principal axes of the ellipsoid is kept parallel to the vorticity vector of the shear flow; in this case the ellipsoid rotates around this axis. The angular rotation and the angular rate of rotation are given by

$$\chi = \tan^{-1}\left(\frac{b}{c}\tan\frac{bcGt}{b^2+c^2}\right), \tag{44}$$

and

$$\dot{\chi} = \frac{G}{b^2+c^2}(b^2\cos^2\chi + c^2\sin^2\chi), \tag{45}$$

respectively, where G is the shear rate and t represents time. In this problem, one of the ellipsoid's principal axes, x, is always parallel to the shear field vorticity vector. This solution also applies to a two-dimensional ellipse (as shown in figure 7) which is the limit of an ellipsoid with one principal axis extended to infinity. From the above analytical solution, it is clear that the motion of the ellipsoid or ellipse is periodic with period

$$T = \frac{2\pi(b^2+c^2)}{bcG}, \tag{46}$$

where in every time interval, T, the particle completes a full rotation.

With fixed density ratio $\alpha = \rho_s/\rho_f = 1.003$, the effect of the Reynolds number on the motion of the particle is discussed by considering the full momentum equation. At $Re = Gd^2/\nu = 0.08$, where $d = 2b$, and the major axis $b = 2c$, the computational domain is 640×320 lattice nodes, $G = 1/256\,00 = 3.906\,25 \times 10^{-5}$ and $b = 16.0$. As mentioned previously (Aidun *et al.* 1997), the computational results agree with Jeffery's solution, as shown in figure 7.

The application is extended to a larger Reynolds number to examine the effect of inertia. With $Re = 0.128$ the results are still close to Jeffery's solution; however, some deviations take place after a few rotations. With $Re \geqslant 1.0$, the results clearly deviate from Jeffery's orbit. The results at $Re > 1$, presented by these simulations, are new to the best of our knowledge. Additional results are presented for Reynolds number, Re, between 5 and 50 in figure 8. The lattice size in this case is 1600×320, and the major axes of the ellipse are $b = 32$ and $c = 16$. The shear rate, therefore, is $G = 1/2048$. As shown in figure 8, for $Re \leqslant 28$ the ellipse rotates in a time-periodic state with non-uniform angular velocity. At $Re \geqslant 30$, however, after the initial transient state, the ellipse eventually reaches a stationary state in the shear field.

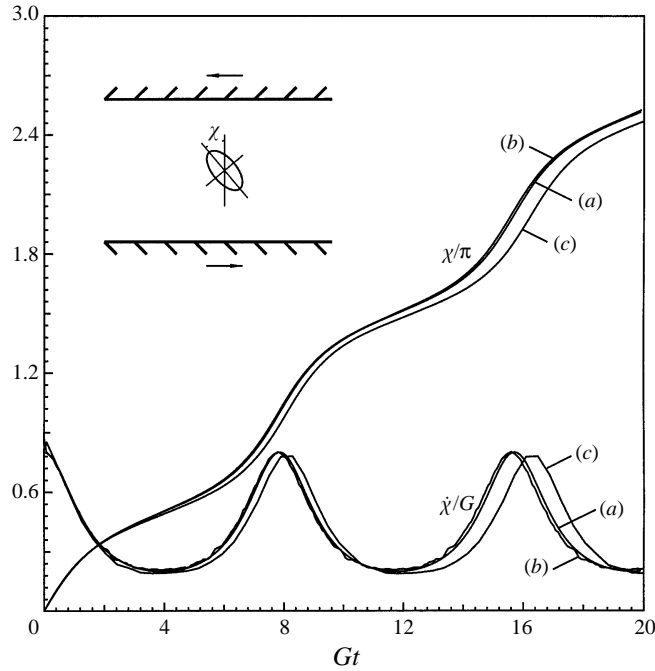It can be seen that the period of rotation increases rapidly with the Reynolds

FIGURE 7. Rotation of an ellipse at small particle Reynolds number. (*a*) Jeffery's solution for $Re = 0$; (*b*) our computational result at $Re = 0.08$; and (*c*) our computational result at $Re = 1.0$. Inset: rotation of an ellipse (i.e. a two-dimensional ellipsoid) $x^2/a^2 + y^2/b^2 + z^2/c^2 = 1$, $1/a \to 0$ in a simple shear flow ($u = 0$, $v = -Gz$, $w = 0$).

number as shown in figure 9. At the critical Reynolds number, ~ 29, the period of oscillation becomes infinitely large. No periodic solution exists beyond this point. The oscillation period varies with Re, as

$$GT = C \times (Re_c - Re)^{-1/2}, \tag{47}$$

where C is a constant. When $C = 100$ and $Re_c = 29$, relation (47) gives a perfect fit to the computational results.

The lattice size is decreased by a factor of two in each direction to ensure that the critical Reynolds number is accurate. The deviations in the solution with the finer lattice size are insignificant.

4.2. *Rotation of an ellipsoid in shear flow*

In this section, the simulations are extended to three-dimensional particles. According to Jeffery's solution (44) and (45), when the system with zero Reynolds number is discussed, there is no difference between the trajectories of a two-dimensional and a three-dimensional particle, since the equation does not include the parameter a. However, when the Reynolds number is no longer zero, the trajectory of a three-dimensional particle will be different from the two-dimensional case. We have analysed the dynamics of ellipsoids with Reynolds numbers up to 90. The semi-axes of the ellipsoid are 16, 16, and 8, and the system size is kept at $40 \times 200 \times 80$. The results are summarized in figures 10 and 11. It is clear that there is a transition at a critical Reynolds number Re_c between 70 and 90. The oscillation period as a function of Reynolds number can be accurately predicted by the scaling law presented by (47)
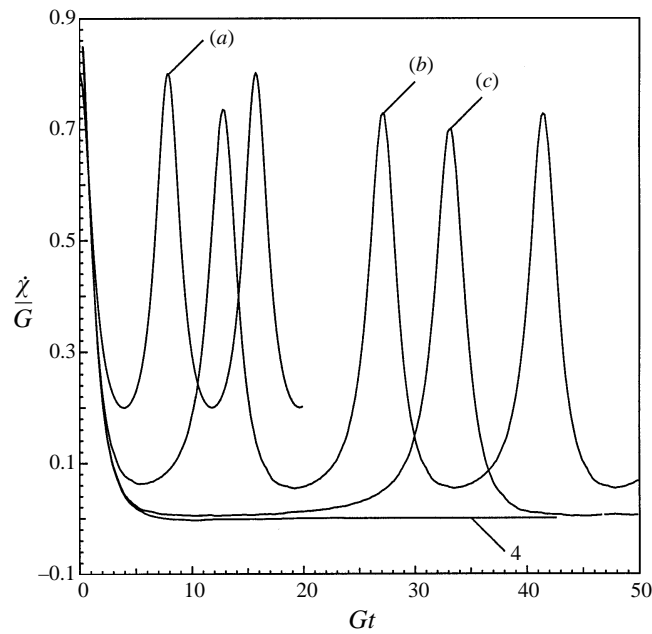
FIGURE 8. The rate of change of the orientation of an elliptic cylinder in a shear field between two parallel channels at various particle Reynolds numbers. (*a*) $Re = 0$; (*b*) $Re = 15$; (*c*) $Re = 28$; and (*d*) $Re = 30$. These results show the lack of existence of the periodic state at $Re \geqslant 30$. $\dot{\chi}$ is the rate of change of angular orientation with time.
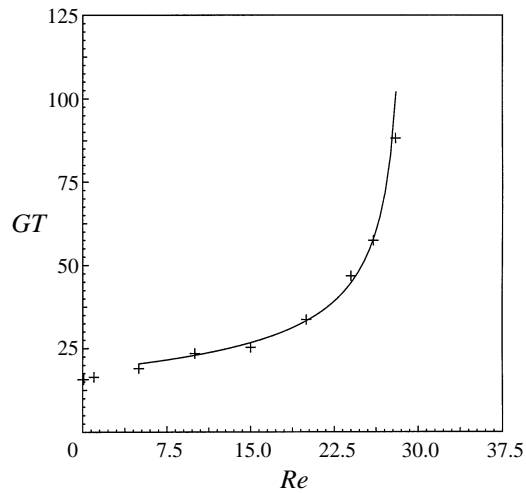

FIGURE 9. The period of the motion of the ellipse increases to infinity as the Reynolds number goes to the critical value. The curve in the figure presents (47) with $C = 100$ and $Re_c = 29$, which is in a good agreement with the simulation results.
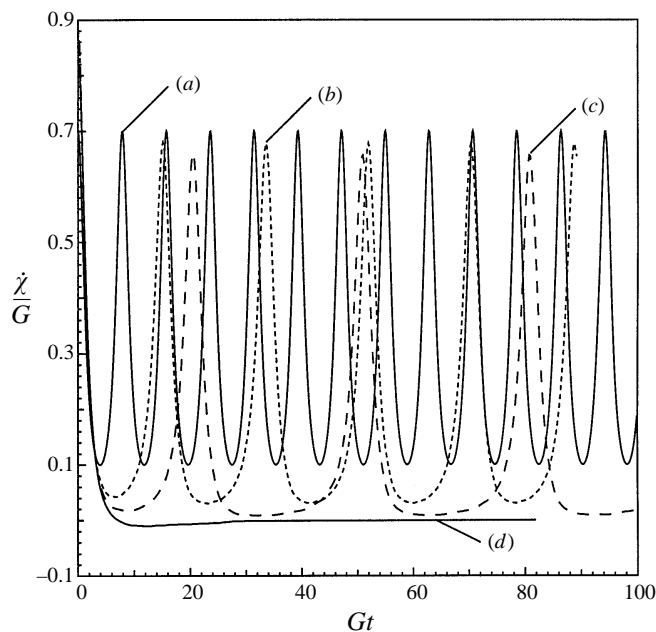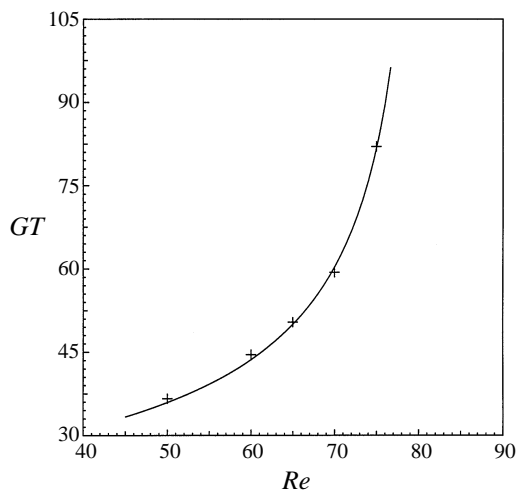
FIGURE 10. Three-dimensional simulation for $\alpha = 1$ with different values of Reynolds numbers.
(*a*) $Re = 0$ (analytical results); (*b*) $Re = 50$; (*c*) $Re = 70$; (*d*) $Re = 90$.

FIGURE 11. The period of the motion of the ellipsoid increases to infinity as the Reynolds number goes to the critical value. The curve in the figure presents (47) with $C = 200$ and $Re_c = 81$, which is in good agreement with the simulation results.

with $C = 200$ and $Re_c = 81$. More details about the dynamics of these systems will be presented elsewhere (Aidun & Ding 1998).

4.3. *Sedimentation of two ellipses in a channel* (*two-dimensional*)

The dynamics of two identical ellipses sedimenting in a long channel shows interesting behaviour. The governing equations for particle motion in fluid are the usual Navier–Stokes and continuity equations complemented by the Newtonian dynamics equation

for the motion of the solid particle. In non-dimensional form, these equations are given by

$$Re \left(\frac{\partial \boldsymbol{u}}{\partial t} + \boldsymbol{u} \cdot \nabla \boldsymbol{u} \right) = -\nabla p + \nabla^2 \boldsymbol{u}, \tag{48}$$

$$\nabla \cdot \boldsymbol{u} = 0, \tag{49}$$

$$\alpha Re \frac{\mathrm{d} \boldsymbol{V}}{\mathrm{d} t} = q^{-1} \boldsymbol{f} + (\alpha - 1) Fr^{-1} Re, \tag{50}$$

where length, velocity, time, and force are scaled by d, U, d/U, and $\mu U d^{n-2}$, respectively. For two-dimensional cases, mass and force are per unit length, and therefore $n = 2$; for three-dimensional cases, $n = 3$. There are four parameters in this equation. These are the Reynolds number, $Re = \rho U d / \mu$, the solid-to-fluid density ratio, $\alpha = \rho_s / \rho$, or the Stokes number, $St = \alpha Re$, the Froude number, $Fr = U^2 / gd$, and the shape parameter, $q = m / \rho_s d^n$, where m is the mass of the solid particle. The Reynolds number and the Stokes number influence the flow more significantly. The magnitude of the hydrodynamic surface force, $\boldsymbol{f}$, and the body force due to buoyancy, the second term on the right-hand side of (50), determine the acceleration and the equilibrium state of the suspended particle. In particle sedimentation problems, as $Re \to 0$, the parameter Re/Fr has to remain finite. When $Re \ll 1$ and $St \ll 1$, then the acceleration terms on the left-hand side can be neglected and the equations reduce to the quasi-steady Stokes equation. Feng & Joseph (1995) studied this sedimentation problem at $Re_p \ll 1$ by direct solution of the steady as well as the unsteady Stokes equation. They show that the results computed from the unsteady Stokes equation are qualitatively different from those from the steady Stokes equations using quasi-steady approximations as in Stokesian Dynamics (Brady & Bossis 1988; Claeys & Brady 1993). In the present calculation, all of the viscous, inertia, and body forces are included. To compare with the results of Feng & Joseph (1995), a case with small Re_p is also considered.

The ellipses have an aspect ratio of 2:1 where the major axis is d. They are released at $t = 0$ from a vertical orientation (i.e. initially the major axis is parallel to the direction of gravity) with initial centre-to-centre distance $2s = d$. The halfway separation point is at the centre of the channel which is a symmetry plane. Similar to Feng & Joseph (1995), we use a computational domain that is $10d$ wide and $25d$ long. The computational domain moves with the particle such that the particles' centres are $10d$ above the bottom boundary. This boundary condition, implemented with the lattice-Boltzmann method, has been outlined above.

The results for centre-to-centre separation and angular rotation for $Re_p = 0.01$, 0.12, 0.47, 1.09, and 6.08 are presented in figures 12(*a–f*), respectively. The particle configuration for these cases is presented in figure 13, and the phase diagram for each case (i.e. plot of angular orientation, θ, vs. particle separation, s) is plotted in figure 14. Here the density ratio, $\alpha = 1.003$, shape factor $q = \frac{1}{8}\pi$, and the Froude number, Fr, depends on the terminal velocity. For small Re_p, the results are compared to finite element computations of Feng & Joseph (1995) in figure 12(*a*) with perfect agreement. The ellipses rotate in a periodic state as they settle inside the channel. With the present results at $Re_p = 0.01$, the weak inertia in the system results in a slight increase in net separation after each cycle. Eventually, the particles drift away from the time-periodic state, represented by a limit cycle at $Re_p = 0$, and approach another time-periodic state. The second limit cycle is qualitatively different since a periodic 'tumbling' motion replaces the 'full somersault' orbit of the particles. This
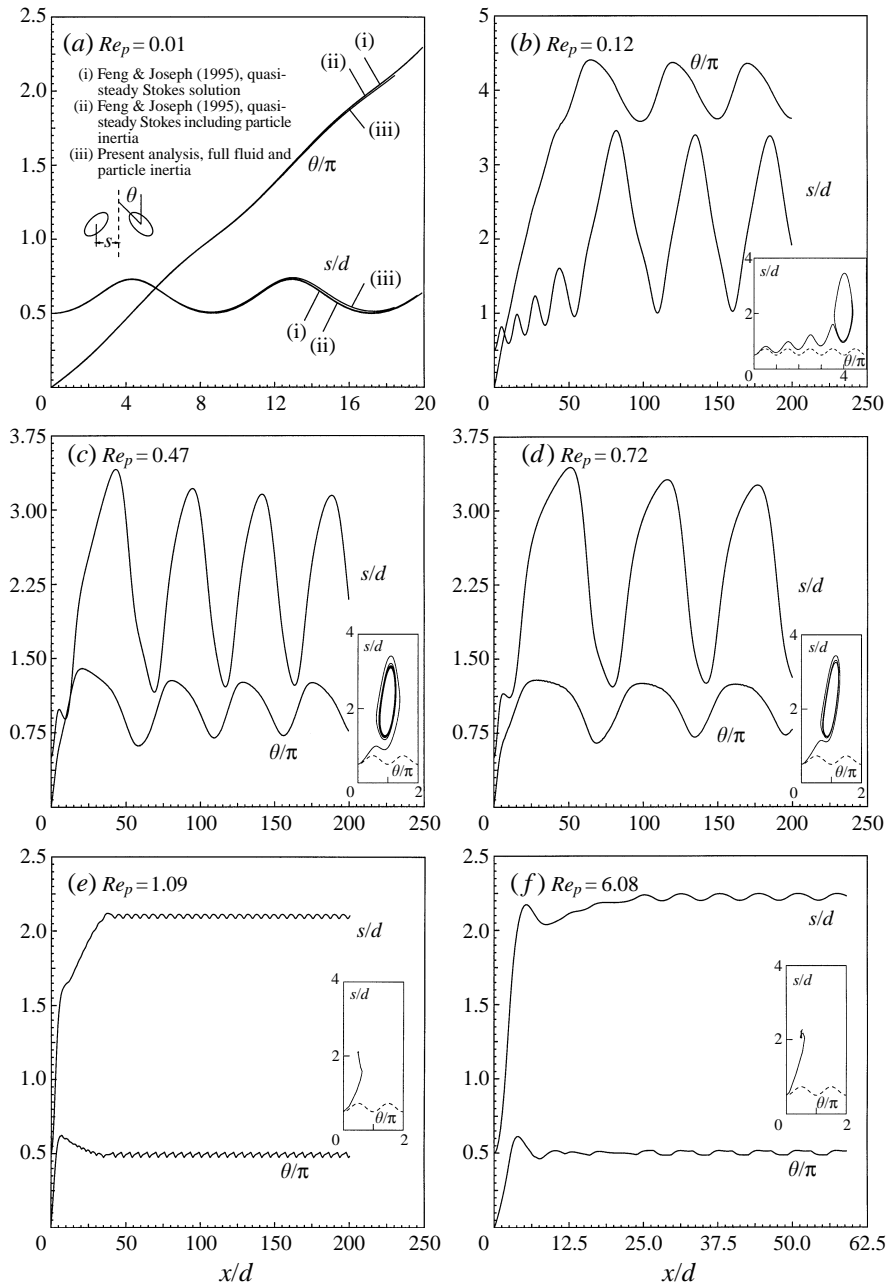
FIGURE 12. Sedimentation of two identical ellipses from initial vertical orientation in an infinitely long vertical channel for Reynolds numbers ranging between 0.01 and 6.08. d is the length of the major axis; s is half of the centre-to-centre separation between the two ellipses; θ is the angle of rotation from the initial configuration; and x is the vertical sedimentation distance from the initial position at $x = 0$. The results obtained by a quasi-steady approximation, neglecting both the fluid inertia and the particle inertia, and the results obtained in absence of fluid inertia, considering just the inertia of solid particles (Feng & Joseph 1995), are also shown in (a).
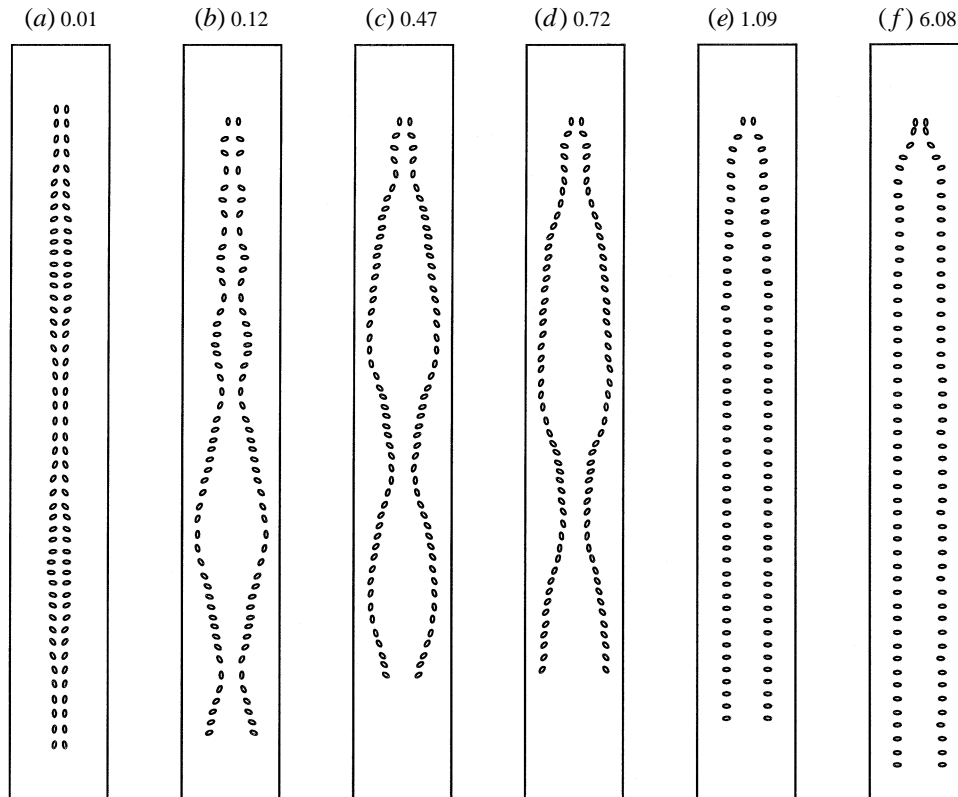
FIGURE 13. Snapshots of the ellipses in time during sedimentation. The Reynolds numbers, from 0.01 to 6.08, specified on the top of each channel, correspond to the Reynolds numbers of the line plots in figure 12.

behaviour can be more clearly observed for the case where $Re_p = 0.12$. The particles go through two complete revolutions while they drift away, as shown in figure 12(b). Eventually, the solution approaches a stable limit cycle at $x/d = 75$ as presented in the phase-space diagram of figure 12(b). At $Re_p = 0.4$–0.7, the particles make only one full revolution before approaching a time-periodic state.

The results suggest the following mechanism. At $Re_p = 0$, the system instantaneously approaches a time-periodic state, T_1, which is a full revolution 'somersault' limit cycle. There is a turning point in the solution at $Re_p = 0$, that is the T_1 state ceases to exist at $Re_p > 0$. This is due to the particle inertia which has a cumulative effect, eventually large enough to prevent full particle rotation.

At Reynolds number about 1 and higher, the particle motion quickly reaches another qualitatively different equilibrium state, as shown in figures 12(e–f) and 13(e–f). The large periodic meandering motion of the particle, seen at smaller Re_p, is suppressed at $Re_p \geqslant 1$. In this range of Reynolds number, we see transitional regions of steady state which exist between various periodic modes. Although this system is rich in dynamics and worth further examination, more detailed analysis is beyond the scope of this paper.
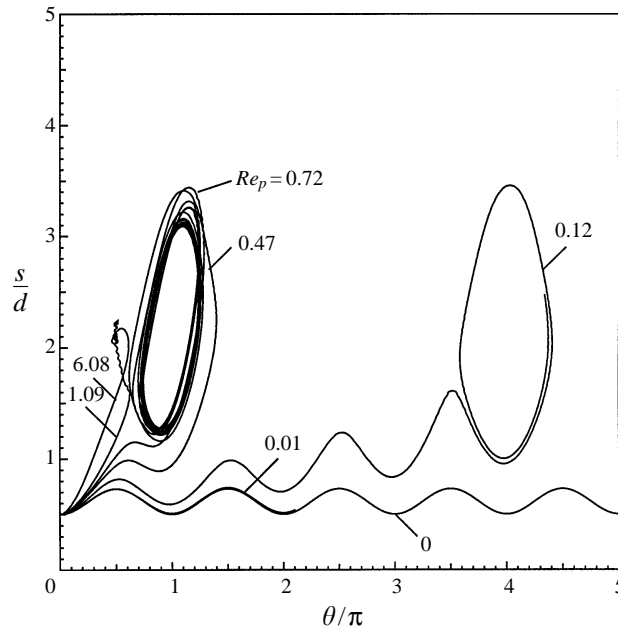
FIGURE 14. Trajectories of the ellipses in phase space, expanded by θ/π and s/d, at various Re_p.

4.4. *Sedimentation of two prolate spheroids in a channel* (*three-dimensional*)

The computational domain for analysis of a pair of prolate spheroids sedimenting in a channel is equal to $25d \times 10d \times 5d$. The computational domain consists of more than 5×10^6 lattice nodes ($400 \times 160 \times 80$) to accurately resolve the flow. The particle Reynolds number is $Re_p = 2.26$ and the other parameters and boundary conditions are the same as in the two-dimensional cases of §4.3. As the solid particles start their descent, they gradually go through a $\pi/2$ rotation and take on a horizontal configuration with a slight amount of wobbling, as shown in figure 15. It is interesting to note that similarly to the two-dimensional case, at larger Reynolds number, the ellipses fall in a horizontal configuration.

5. Concluding remarks

The present method has been developed because of the limited applicability of the previous methods (Hu *et al.* 1992; Feng *et al.* 1994; and Ladd 1994*a,b*) for hydrodynamic analysis of particles suspended in fluid. The computational methods based on the solution of the discrete Boltzmann equation are considerably more efficient compared to the finite element simulation solutions of the Navier–Stokes equations. The method presented here removes the limitations of the previous discrete Boltzmann approach and applies to any solid-to-fluid density ratio. Also, the present method applies to oscillating solid particles with any frequency without a need for parameter adjustments.

The shortcoming of the current method is that the operator in (26) for solid boundary nodes is not mass conservative. Besides, as discussed in §2.4, when a fluid node is covered by a moving solid particle, the fluid at this node will be removed from the system. On the other hand, when a fluid node previously occupied by a solid particle is recovered, the fluid density at this newly created node is assumed to
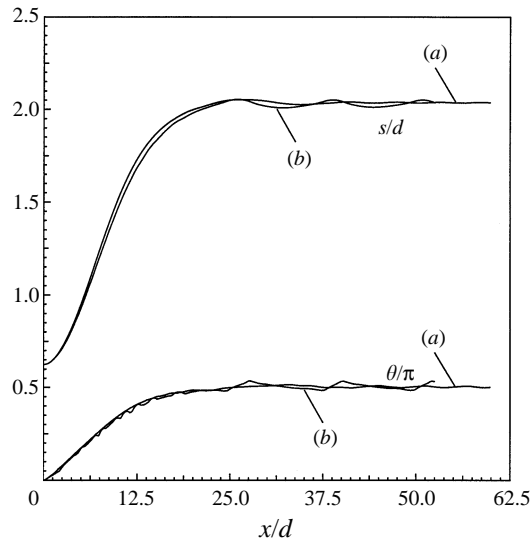
FIGURE 15. Sedimentation of two identical prolate spheroids from initial vertical orientation in an infinitely long vertical channel for Reynolds number 2.26. The computational domain is $25d \times 10d \times 5d$ discretized by $400 \times 160 \times 80$ (*a*) or $200 \times 80 \times 40$ (*b*) nodes.

be the average of the fluid density of the nneighbouring nodes. The local fluid mass, therefore, is not conservative. However, the effect of this numerical inconsistency is insignificant, and less than numerical noise in the computations. The total average mass in the macroscopic level is conserved. Further improvement of the method is under investigation.

This method has been implemented on parallel processors where the code is very effective for three-dimensional simulations. Using the parallel programming code with a Message Passing Interface (MPI) the computational time for completing the calculations in §4.2 with 640 000 nodes and $Re = 70$ from $Gt = 0$ to 100 consisting of 51 200 time steps using 16 parallel processors is about 3.5 hours. With a Parallel Virtual Machine (PVM) facility the computational time for analysis of particle sedimentation in §4.4 with 5 120 000 nodes from $x/d = 0$ to 75 consisting of 16 800 time steps using 64 processors is about 6 hours.

REFERENCES

AIDUN, C. K. & LU, Y. 1995 Lattice Boltzmann simulation of solid particles suspended in fluid. *J. Statist. Phys.* **81**, 49.

AIDUN, C. K., LU, Y. & DING, E. 1997 Dynamic simulation of particles suspended in fluid. *The 1997 ASME Fluids Engineering Division Summer Meeting, (FEDSM'97), June 22–26*.

AIDUN, C. K. & DING, E. 1998 Dynamic simulation of an ellipsoid particle suspended in shear flow (in preparation).

BRADY, J. F. & BOSSIS, G. 1988 Stokesian Dynamics. *Ann. Rev. Fluid Mech.* **20**, 111.

CHEN, H., CHEN, S. & MATTHAEUS, W. H. 1992 Recovery of the Navier–Stokes equations using a lattice-gas Boltzmann method. *Phys. Rev.* A **45**, R5339.

CLAEYS, I. L. & BRADY, J. F. 1993 Suspensions of prolate spheroids in Stokes flow. Part 1. Dynamics of a finite number of particles in an unbounded fluid. *J. Fluid Mech.* **251**, 411.

FENG, J., HU, H. H. & JOSEPH, D. D. 1994a Direct simulation of initial value problems for the motion of solid bodies in a Newtonian fluid. Part 1. Sedimentation. *J. Fluid Mech.* **261**, 95.

FENG, J., HU, H. H. & JOSEPH, D. D. 1994b Direct simulation of initial value problems for the motion of solid bodies in a Newtonian fluid. Part 2. Couette and Poiseuille flows. *J. Fluid Mech.* **277**, 271.

FENG, J. & JOSEPH, D. D. 1995 The unsteady motion of solid bodies in creeping flows. *J. Fluid Mech.* **303**, 83.

HOU, S., ZOU, Q., CHEN, S., DOOLEN, G. & COGLEY, A. C. 1995 Simulation of cavity flow by lattice Boltzmann method. *J. Comput. Phys.* **118**, 329.

HU, H. H. 1996 Direct simulation of flows of solid-liquid mixtures. *Intl J. Multi-phase Flow* **22**, 335.

HU, H. H., CROCHET, M. J. & JOSEPH, D. D. 1992 Direct simulation of fluid particle motions. *Theor. Comput. Fluid Dyn.* **3**, 285.

HUANG, Y., FENG, J. & JOSEPH, D. D. 1994 The turning couple on an elliptic particle settling in a vertical channel. *J. Fluid Mech.* **271**, 1.

JEFFERY, G. B. 1922 The motion of ellipsoidal particles immersed in a viscous fluid. *Proc. R. Soc. Lond.* A **102**, 161.

JOSEPH, D. D. 1994 Interrogation of numerical simulation for modeling of flow induced microstructure. In *Liquid-Solid Flows*, vol. 189, p. 31. ASME.

LADD, A. J. C., COLVIN, M. E. & FRENKEL, D. 1988 Application of lattice-gas cellular automata to the Brownian motion of solids in suspension. *Phys. Rev. Lett.* **60**, 975.

LADD, A. J. C. 1994a Numerical simulations of particulate suspensions via a discretized Boltzmann equation. Part 1. Theoretical foundation. *J. Fluid Mech.* **271**, 285.

LADD, A. J. C. 1994b Numerical simulations of particulate suspensions via a discretized Boltzmann equation. Part 2. Numerical results. *J. Fluid Mech.* **271**, 311.

LOWE, C. P., FRENKEL, D. & MASTERS, A. J. 1995 Long-time tails in angular momentum correlations. *J. Chem. Phys.* **103**, 1852.

MCNAMARA, G. R. & ZANETTI, G. 1988 Use of the Boltzmann equation to simulate lattice-gas automata. *Phys. Rev. Lett.* **61**, 2332.

MIYAMURA, A., IWASAKI, S. & ISHII, T. 1981 Experiment wall correction factors of single solid spheres in triangular and square cylinders, and parallel plates. *Intl J. Multi-phase Flow* **7**, 41.